



# Synthesis of titanium dioxide-based electrocatalysts using in-liquid plasma method for carbon dioxide reduction and hydrogen formation

Kai Takagi<sup>a,b</sup>, Yuvaraj M. Hunge<sup>c</sup>, Izumi Serizawa<sup>b</sup>, Chiaki Terashima<sup>a,c,\*</sup>

<sup>a</sup> Graduate School of Science and Technology, Tokyo University of Science, 2641 Yamazaki, Noda, Chiba 278-8510, Japan

<sup>b</sup> ORC Manufacturing Co., Ltd., 4896 Tamagawa, Chino, Nagano 391-0011, Japan

<sup>c</sup> Research Institute for Science and Technology, Tokyo University of Science, 2641 Yamazaki, Noda, Chiba 278-8510, Japan

## ARTICLE INFO

**Keywords:**  
Electrochemistry  
Redox  
Electrode  
Syngas  
Fuel

## ABSTRACT

This study explores TiO<sub>2</sub>-based electrocatalysts for CO<sub>2</sub> reduction using an innovative in-liquid plasma method. The plasma technique allowed Cu, Ag, and W to be deposited on TiO<sub>2</sub>, enhancing its electrocatalytic properties. Ag/Ag<sub>2</sub>O core-shell nanoparticles were synthesized on Ag rod electrodes, and the Faraday efficiency of CO in electrocatalytic CO<sub>2</sub> reduction reached 50 %. For Cu electrodes, the oxidation state of Cu particles varied with the solution composition, impacting product yields. In HNO<sub>3</sub> solution, CH<sub>4</sub> (50 μmol) and C<sub>2</sub>H<sub>4</sub> (3.3 μmol) were produced, which was 1.2 times that of NH<sub>4</sub>OH and KCl solution. XPS showed that the proportion of Cu<sup>2+</sup> in the HNO<sub>3</sub> solution increased slightly. These findings underscore the critical role of metal oxidation states and plasma treatment in product distribution. Overall, this study demonstrates that in-liquid plasma can reduce catalyst loading, maintain high Faraday efficiency, and has scalable potential for industrial CO<sub>2</sub> reduction applications.

## 1. Introduction

Recently, in an effort to reduce greenhouse gases in line with the Sustainable Development Goals (SDGs), research has focused on collecting carbon dioxide (CO<sub>2</sub>) from the atmosphere and converting it into a useful resource [1,2]. Among various methods, the conversion of CO<sub>2</sub> using electrocatalysts stands out from an industrial perspective because it can be carried out at room temperature and pressure [3]. Unlike conventional electrodes impregnated with solution, this method employs a gas diffusion electrode (GDE) that reacts at the gas-liquid interface, significantly improving conversion efficiency [4]. Typically, a GDE consists of three layers: a gas diffusion layer (GDL) made of hydrophobically treated carbon fiber with polytetrafluoroethylene (PTFE), conductive carbon black (CB) mixed with PTFE, and a catalyst layer (CL) made of CB loaded with a catalyst [5,6]. Designing a highly efficient GDE is complex, requiring considerations such as the hydrophobic treatment and aperture ratio of the GDL, the flow path design of the terminal electrode, and the hydrophobicity of the catalyst layer [7]. Importantly, the catalyst in the catalyst layer is crucial for the efficient reduction of CO<sub>2</sub> to the desired product. The catalyst layer is supported by various metals such as Au, Ag, Cu, Pb, and Sn on the CB. These supported metals are broadly classified into three categories based on

the reduction products they yield: carbon monoxide (CO), formic acid (HCOOH), and hydrocarbons [8,9]. Among them, Cu stands out due to its unique adsorption behavior on the intermediate products of CO<sub>2</sub> reduction, forming hydrocarbon compounds [10]. The catalyst layer can be formed by either sputtering metal directly onto the GDL of the GDE [11] or by supporting metal nanoparticles on the CB of the CL using a liquid-phase reduction method [12]. In the sputtering method, metal nanoparticles are supported by generating plasma between the GDE and the metal in a vacuum atmosphere. This method is straightforward as GDEs can be used directly. However, there are concerns about damage to the GDE caused by plasma, and scaling up requires larger equipment and higher costs. The liquid-phase reduction method supports metal nanoparticles on CB by reducing metal ions in solution. While this method can synthesize large amounts of powdered electrocatalysts with controllable size and crystallinity of metal nanoparticles, it has a significant environmental impact due to the chemicals used and the treatment of metal ions. Therefore, a new electrocatalyst synthesis method that can produce large amounts of electrocatalysts with a low environmental impact is desirable.

Recently, methods for synthesizing nanoparticles using in-liquid plasma have been investigated [13]. In-liquid plasma is generated by applying microwaves or high-frequency/high-voltage to electrodes in a

\* Corresponding author at: Graduate School of Science and Technology, Tokyo University of Science, 2641 Yamazaki, Noda, Chiba 278-8510, Japan.  
E-mail address: [terashima@rs.tus.ac.jp](mailto:terashima@rs.tus.ac.jp) (C. Terashima).

<https://doi.org/10.1016/j.jece.2024.115242>

Received 17 August 2024; Received in revised form 18 November 2024; Accepted 26 December 2024

Available online 27 December 2024

2213-3437/© 2024 Elsevier Ltd. All rights reserved, including those for text and data mining, AI training, and similar technologies.

solution with controlled electrical conductivity. The process involves: 1) applying high-frequency/high-voltage to the electrodes, 2) Joule heating the liquid between the electrodes, 3) forming bubbles due to Joule heating, and 4) generating plasma within the bubbles through high frequency and high voltage. In-liquid plasma can create plasma in a solution where the powder is dispersed, enabling the support of nanoparticles on the powder. Additionally, the plasma creates a high-temperature, highly active reaction field, which is expected to modify both the dispersed powder and the produced nanoparticles.

In our previous work, we investigated titanium dioxide (TiO<sub>2</sub>) as an alternative material to conductive carbon black (CB) for use as the catalyst support in electrocatalytic CO<sub>2</sub> reduction by applying liquid plasma to TiO<sub>2</sub> [14]. We found that tungsten (W) derived from electrodes in liquid plasma is dispersed in TiO<sub>2</sub>, and that the amount of hydrogen production can be controlled by W, which promotes hydrogen production. In this study, plasma in liquid was generated using the various electrodes and solutions to synthesize new efficient catalysts for electrocatalytic CO<sub>2</sub> reduction. Catalysts were synthesized using various types of various in-liquid plasma electrode rods, and the contribution to the selectivity of the reduction products in electrocatalytic CO<sub>2</sub> reduction was evaluated. In addition, the oxidation state of the catalyst was evaluated by synthesizing the catalyst using acidic, neutral, and alkaline solutions as the solution for the in-liquid plasma. Finally, we considered the effect on the selectivity in electrocatalytic CO<sub>2</sub> reduction.

## 2. Experiment

### 2.1. Materials

For this study, all chemicals employed in in-liquid plasma treatment, electrochemical characterization, catalyst loading, and CO<sub>2</sub> electro-reduction were used as received. Copper (Cu, 99.9 %, Nilaco), silver (Ag, 99.99 %, Nilaco), and tungsten (W, 99.95 %, Nilaco) rods with a 3 mm diameter were used for the in-liquid plasma electrodes. The chemicals used include ammonia aqueous solution (30 wt%-NH<sub>4</sub>OH, Wako), P25 (TiO<sub>2</sub>, Aeroxide), carbon black (Vulcan XC 72, Fuel Cell Store), Nafion dispersion (5 wt%-Nafion Dispersion Solution, Wako), isopropanol ((CH<sub>3</sub>)<sub>2</sub>CHOH, 99.7 %, Wako), potassium hydroxide (KOH, Wako), potassium chloride (KCl, Wako), and nitric acid (60 wt%-HNO<sub>3</sub>, Wako). Gases such as N<sub>2</sub> (99.99995 vol%, Taiyo Nippon Sanso) and CO<sub>2</sub> (99.995 vol%, Taiyo Nippon Sanso) were used during the investigation of electrochemical properties. H<sub>2</sub> (99.99 %, GL Sciences), CO, CH<sub>4</sub>, and C<sub>2</sub>H<sub>4</sub> (99.9 %, GL Sciences) were used to identify and quantify the CO<sub>2</sub> reduction products. Each solution was prepared using deionized water with a resistivity of approximately 18 MΩ/cm.

### 2.2. In-liquid plasma treatment of TiO<sub>2</sub> using various metal electrodes

The in-liquid plasma system consisted of a custom-made quartz tube used as a reaction vessel (see [supplementary material](#)). Ag, Cu, or W bar electrodes were inserted into the quartz tube, with opposing electrodes set 2 mm apart. Each metal rod electrode was covered with an insulating tube (5 mm diameter) to avoid unwanted contact with the solution, with the tip exposed about 1.5 mm. 0.5 g of P25 was dispersed in 200 mL of 5 wt%-NH<sub>4</sub>OH solution and constantly cooled using a cooler set at 0°C. The dispersion was stirred and circulated by a magnetic stirrer and peristaltic pump at 200 rpm and 180 rpm, respectively. Plasma was generated using a bipolar pulse power supply (MPP04-A4-200, Kurita) at an applied voltage of 4 kV, frequency of 100 kHz, and pulse width of 0.5 μs for 2 h. The emission spectrum of the in-liquid plasma was measured through the quartz tube near the plasma generator using a plasma process monitor (C7460, Hamamatsu Photonics). The voltage and current waveforms of the plasma in liquid were evaluated using a digital oscilloscope (TBS1052B, Tektronix). The treated solution was centrifuged (3700, Kubota Corporation) at 15,000 rpm for 1 h and then washed twice with deionized water. After suction filtration, the product

was dried in a vacuum dryer set at 80°C for 1 h. The resulting solid material was powdered in an agate mortar. P25 treated with Ag, Cu, or W bar electrodes were designated as Ag-P25, Cu-P25, and W-P25, respectively.

To evaluate the amount of nanoparticles loaded relative to the amount of P25 prepared, P25 was varied to 1.0 g and 2.0 g under the Cu rod electrode conditions. These were designated as Cu-1.0 and Cu-2.0. For comparison with P25, CB was used as a catalyst support and subjected to liquid plasma treatment with Ag and Cu rod electrodes, resulting in Ag-CB and Cu-CB. To investigate the effect of solution composition on nanoparticle synthesis using liquid plasma, KCl or HNO<sub>3</sub> solutions were used instead of the 5 wt%-NH<sub>4</sub>OH solution. The concentrations of these solutions were adjusted to achieve the same electrical conductivity (1.3 mS/cm) as the 5 wt%-NH<sub>4</sub>OH solution, as the electrical conductivity of the solution significantly affects the in-liquid plasma [15,16]. The metal bar electrode was made of Cu and treated with P25 liquid plasma under the above conditions to produce Cu-KCl and Cu-HNO<sub>3</sub>. The pHs of 5.0 wt%-NH<sub>4</sub>OH, 1.3 mS/cm-KCl and 1.3 mS/cm-HNO<sub>3</sub> were 12.02, 5.64 and 2.51, respectively. The particle shape and elemental composition of the prepared powder were evaluated by scanning electron microscopy (JSM-7600F, JEOL Ltd.). The crystal structure was assessed using powder X-ray diffraction (Ultima IV, Rigaku Co., Ltd.) with a Cu-Kα wavelength (λ = 1.5406 Å), a current of 40 mA, a voltage of 40 kV, and a 2θ range from 20° to 80°. Crystal lattice constants were calculated by Rietveld analysis using reference data. Interfacial binding states were evaluated by X-ray photoelectron spectroscopy (XPS) (AXIS-NOVA SP, KRATOS Analytical Ltd.). The XPS apparatus was operated using Al-Kα (λ = 8.3412 Å) as the X-ray source, with a current of 10 mA and a voltage of 15 kV. Each element's peak was calibrated using the C 1 s peak (284.8 eV).

### 2.3. Electrocatalytic CO<sub>2</sub> reduction characterizations

The working electrode was fabricated by applying electrode ink onto a gas diffusion layer (GDL) with a microporous layer (Toray Carbon Paper 060 with Micro Porous Layer, Fuel Cell Store, 15 × 15 mm), achieving a catalyst loading of 1.0 mg/cm<sup>2</sup>. The electrode ink was prepared by mixing 2.44 mL each of isopropanol and deionized water, adding 20 mg of the powder sample, and 120 μL of Nafion dispersion, then sonicating the mixture for 30 min. For the working electrode, the fabricated gas diffusion electrode (GDE) was cut into a 1/4 square, and Cu tape was attached to the four sides of the GDL for electrical continuity.

The gas diffusion cell is a three-chamber cell consisting of gas, cathode, and anode compartments, as previously reported (see [supplementary material](#)). The working electrode was placed between the gas phase and the cathode liquid using a spacer with an 8 mm diameter hole, resulting in an electrode area of 0.5 cm<sup>2</sup>. Platinum mesh was used as the counter electrode, Hg/HgO (RE-61AP, BAS) was used as the reference electrode, and 50 mL of 1.0 M-KOH (pH = 13.5) was used as the electrolyte for both the anode and cathode. The anode and cathode compartments were separated by a proton exchange membrane (Nafion-212, Sigma-Aldrich). The electrolyte was pumped into the cathode and anode chambers at a rate of 5 mL/min using a peristaltic pump. The cathode and anode chambers each had a volume of 8 mL. CO<sub>2</sub> gas was purged into the gas chamber at a rate of 15 mL/min, and the product gas was collected using a sampling bag. Electrocatalytic CO<sub>2</sub> reduction was performed for 10 min at current densities of -50, -125, -250, and -500 mA/cm<sup>2</sup> using chronopotentiometry. The gas diffusion cell was operated using a potentiostat/galvanostat instrument (ModuLab XM ECS, Solartron Analytical). The observed potentials were converted to a reversible hydrogen electrode (RHE) reference using Eq. (1).

$$E(\text{V vs. RHE}) = E(\text{V vs. Hg/HgO}) - 0.059 \times \text{pH} - E_{\text{Hg/HgO}}(\text{V vs. SHE}) \quad (1)$$

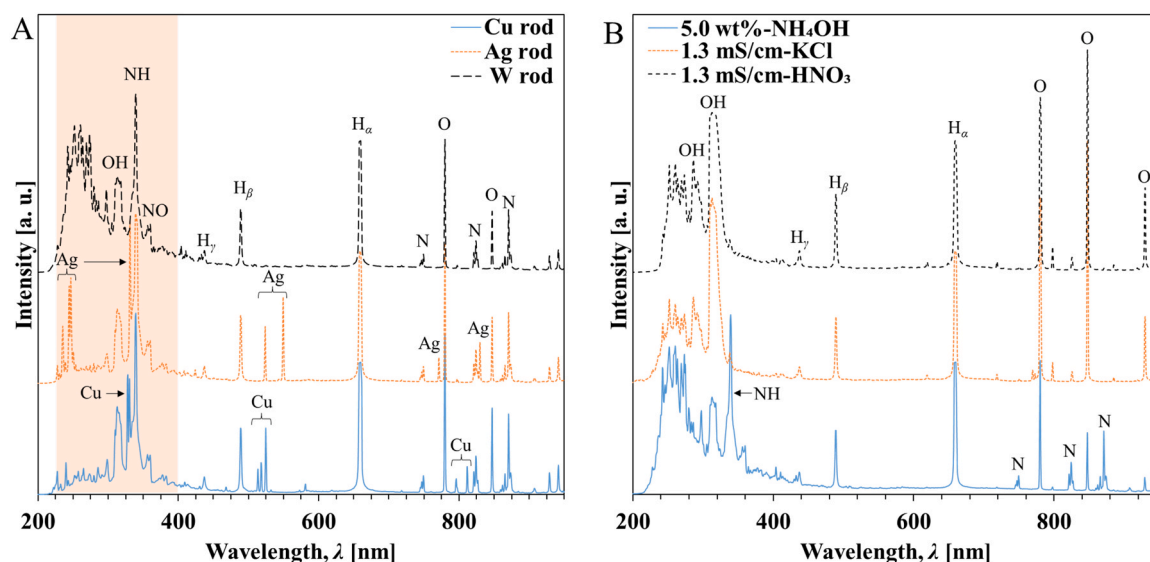


**Fig. 1.** Emission spectra of in-liquid plasma when using Cu, Ag and W rod electrode in 5.0 wt%-NH<sub>4</sub>OH (A), and in solutions 5.0 wt%-NH<sub>4</sub>OH, 1.3 mS/cm-KCl and 1.3 mS/cm-HNO<sub>3</sub> with W rod electrode (B).

E(V vs. RHE) and E(V vs. Hg/HgO) represent the potentials with respect to the RHE and Hg/HgO electrodes, respectively. E<sub>Hg/HgO</sub>(V vs. SHE) shows the potential of the Hg/HgO electrode with respect to a standard hydrogen electrode (0.199 V vs. SHE). The collected gas samples were measured by gas chromatography (GC2014, Shimadzu) equipped with a Hydrogen flame Ionization Detector (FID) connected with a methanizer (MTN-1, Shimadzu) and Thermal Conductivity Detector (TCD) for CO, CH<sub>4</sub> and C<sub>2</sub>H<sub>4</sub>, and H<sub>2</sub>, respectively. FID was performed using a Shincarbon-ST 50/80 mesh column made by Shinwa Chem. Ins. Ltd. using He as carrier gas, and TCD was performed using Molecular Sieve 5 A 60/80 mesh made by GL Sci. Inc. using Ar as a carrier gas. The reduction products were used to calculate Faraday efficiency (FE) using Faraday's second law in Eq. (2).

$$FE(\%) = nzF/Q \times 100 \quad (2)$$

where *n* and *z* are the number of moles and electrons of the product, respectively; *F* is Faraday constant (96,485 C/mol); and *Q* is the total charge (C) of the electrocatalytic CO<sub>2</sub> reduction. The electrocatalytic CO<sub>2</sub> reduction properties were evaluated three times for each electrode.

### 3. Results and discussion

#### 3.1. Morphological and structural characterizations

Fig. 1 shows the emission spectra of in-liquid plasma generated using each metal bar electrode and plasma in liquid generated using the W bar electrode (the emission spectra of plasma in liquid for each condition are shown in [supplementary material](#)). From Fig. 1 A, metal-derived emission spectra were observed at 324, 327, 510, 515, 521, 796, and 811 nm for the Cu rod electrode, and at 235, 244, 523, 549, 771, and 829 nm for the Ag rod electrode [17,18]. W exhibited a broad peak from 225 nm to 400 nm. No clear bright lines were identified in the emission spectrum of W. This is because W has a much higher melting point than other common metals and almost no luminescence occurs due to atomic transitions [19]. Consequently, each metal rod electrode dissolved into the solution. Fig. 1 B shows the emission spectrum of the plasma in liquid for each solution using a W bar electrode. The 5.0 wt%-NH<sub>4</sub>OH solution showed strong emission spectra originating from NH at 339 nm and N at 750, 824, and 870 nm due to the higher concentration of

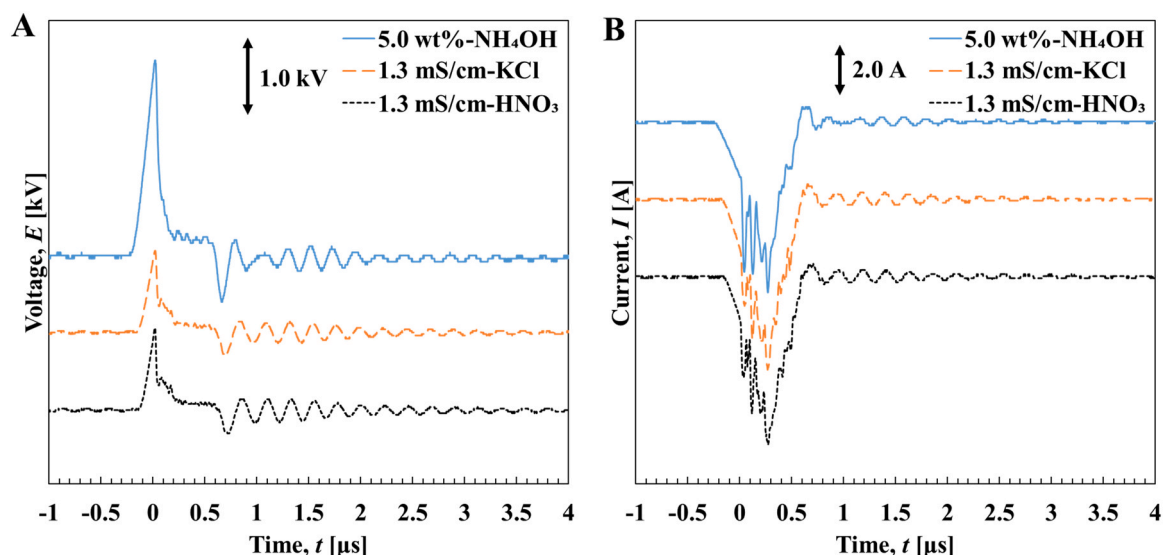


**Fig. 2.** Voltage (A) and current (B) waveforms of in-liquid plasma in 5.0 wt%-NH<sub>4</sub>OH, 1.3 mS/cm-KCl and 1.3 mS/cm-HNO<sub>3</sub> solution with W rod electrode.

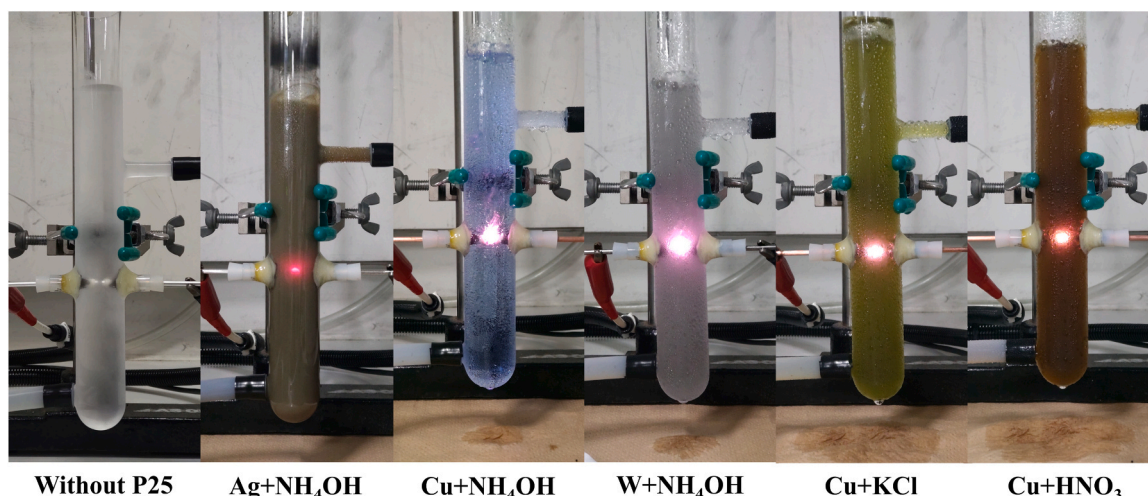


Fig. 3. Photographs of before plasma generation without P25, and after 2 h treatment Ag+NH<sub>4</sub>OH, Cu+NH<sub>4</sub>OH, W+NH<sub>4</sub>OH, Cu+KCl, and Cu+HNO<sub>3</sub>.

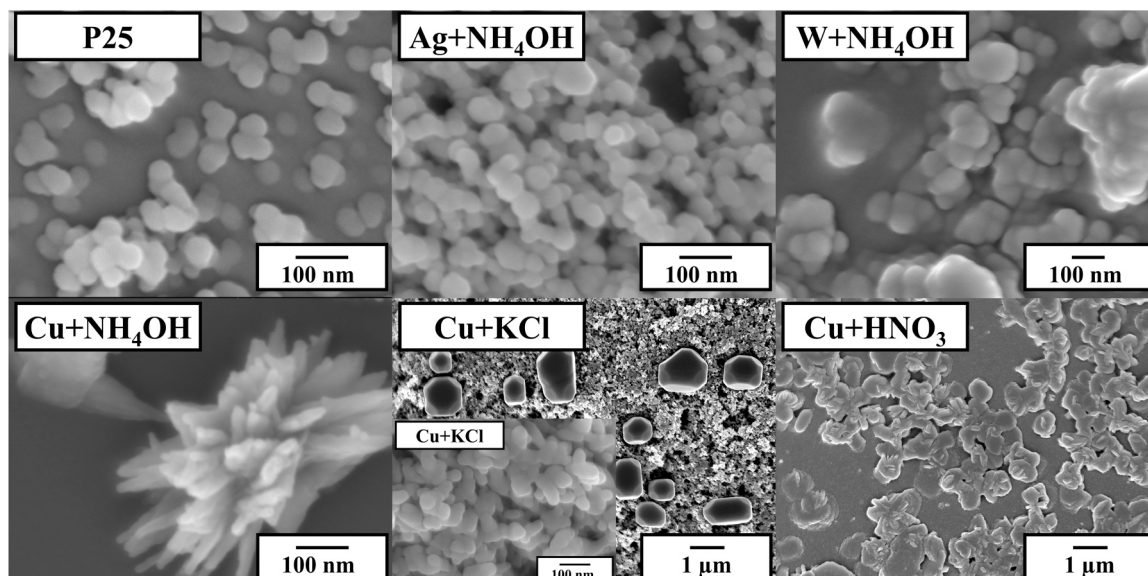


Fig. 4. SEM images of P25 and each after 2 h in-liquid plasma treatment solution dried on a Si substrate.

NH<sub>4</sub>OH compared to the other solutions [20,21]. In addition, the emission spectra derived from oxygen (O) at 780, 847, and 929 nm decreased, and those derived from hydrogen (H) at 438, 489, and 659 nm increased [22,23]. These observations indicate that the major component of the plasma is NH<sub>4</sub>OH. For KCl and HNO<sub>3</sub>, no emission spectra were observed for the respective solution components [24,25]. Assuming similar conductivity concentrations, it is inferred that the concentrations of these components were very low, resulting in their absence from the emission spectrum. The emission spectra suggest that the composition of the solution can be varied to create highly reactive reaction fields rich in oxidation and reduction.

The voltage-current waveforms for each solution showed a peak voltage of 2.5 kV only for the 5.0 wt%-NH<sub>4</sub>OH solution (Fig. 2 A). The 1.3 mS/cm-HNO<sub>3</sub> and 1.3 mS/cm-KCl solutions exhibited similar peak voltages. Peak currents were approximately 6 A for all conditions (Fig. 2 B). After the breakdown of the gas, the plasma transitioned between glow discharge and arc discharge states [26]. This led to dielectric breakdown at peak voltages and an increase in current. Based on the relationship between voltage and current, it is inferred that this corresponds to a glow discharge. The voltage and current waveforms for each metal bar electrode are shown in [supplementary material](#). As mentioned

above, luminescence was observed in the 5.0 wt%-NH<sub>4</sub>OH solution due to the higher NH<sub>4</sub>OH concentration. It is therefore inferred that the increased voltage requirement was due to the need to generate plasma by dissociating H<sub>2</sub>O and NH<sub>4</sub>OH. The upper limit of the current peak is determined by the device's output capacity relative to the voltage. The power supply used in this study had a current limit of 6 A, with safety devices activating above this threshold.

To observe changes in the solutions where liquid plasma was generated, photographs were taken of each solution after in-liquid plasma treatment without the addition of P25 (Fig. 3). The solutions were then dried and observed by SEM (Fig. 4). Changes in the solutions over time under each condition are shown in [supplementary material](#). The solution in which in-liquid plasma was generated at the Ag rod electrode turned black-grey and turbid. In contrast, the solution with in-liquid plasma generated at the Cu rod electrode appeared clear dark-blue, likely due to the dissolution of Cu, forming a complex with NH<sub>4</sub>OH. Cu<sup>2+</sup> ions in aqueous solution typically exhibit a characteristic blue color. However, the solution obtained with plasma generated at the Cu rod electrode showed a light blue color, likely due to the dissolution of Cu, forming a complex with NH<sub>4</sub>OH. After checking the details, the colored solution was found to have a strong absorption at around

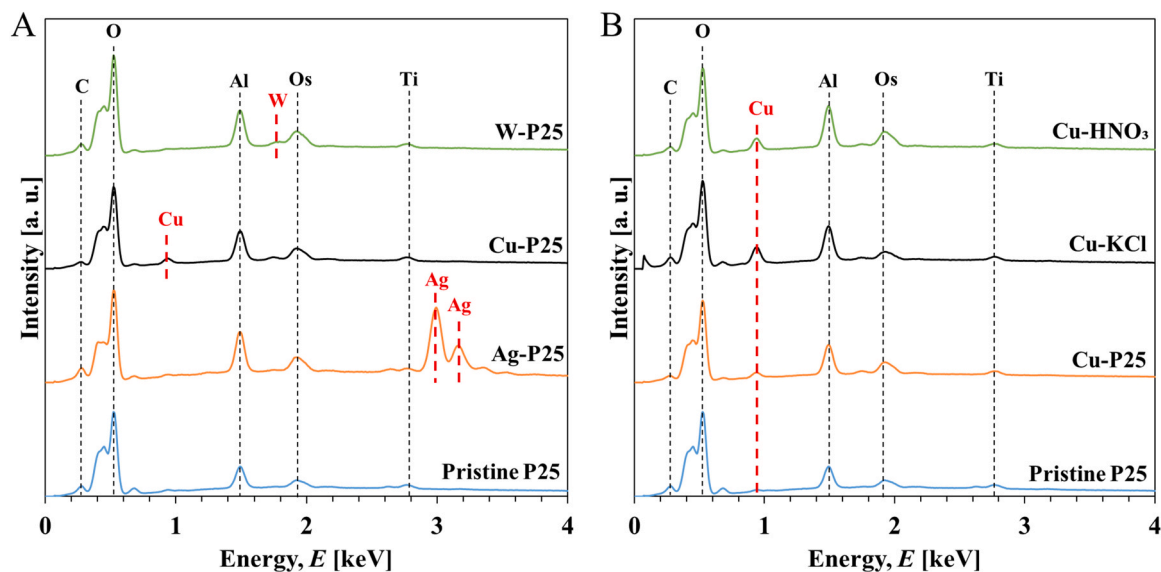


Fig. 5. EDS spectra of P25, Ag-P25, Cu-P25 and W-P25 (A), and P25, Cu-P25, Cu-KCl and Cu-HNO<sub>3</sub> (B).

Table 1

Etching volume of electrode rod and ratio of powder under various experimental conditions.

Powder	Weight [g]	Solution	Electrode rod	Etching volume [g]	Weight ratio of electrode rod metal to powder [wt%]	Weight ratio of electrode rod metal to powder calculated from EDS [wt%]
P25	0.50	NH <sub>4</sub> OH	Ag	0.097	16.2	9.8
P25	0.50	NH <sub>4</sub> OH	Cu	0.038	7.1	1.3
P25	1.00	NH <sub>4</sub> OH	Cu	0.048	4.6	1.3
P25	2.00	NH <sub>4</sub> OH	Cu	0.034	1.7	1.2
P25	0.50	KCl	Cu	0.029	5.4	4.7
P25	0.50	HNO <sub>3</sub>	Cu	0.038	7.1	3.3
P25	0.50	NH <sub>4</sub> OH	W	0.041	7.6	0.5
CB	0.50	NH <sub>4</sub> OH	Ag	0.085	14.5	7.6
CB	0.50	NH <sub>4</sub> OH	Cu	0.048	8.8	0.1

620 nm, and the peak was in the same position as the adjusted 10 mmol-[Cu(NH<sub>3</sub>)<sub>4</sub>]<sup>2+</sup> (see [supplementary materials](#)). The W rod electrode solution turned light grey, while the KCl solution of the Cu rod electrode became brownish-green, and the HNO<sub>3</sub> solution of the Cu rod electrode turned cloudy reddish-brown. The form of Cu species is known to depend on pH. Cu species exist as Cu<sup>2+</sup> in HNO<sub>3</sub>, Cu<sup>2+</sup> and Cu(OH)<sup>+</sup> in KCl, Cu(OH)<sub>2</sub> and Cu(OH)<sub>2</sub><sup>+</sup> in NH<sub>4</sub>OH, and Cu(OH)<sub>3</sub> in NH<sub>4</sub>OH [27]. It is thought that the surface of the Cu particles was oxidized by HNO<sub>3</sub>, causing them to turn reddish brown. In the KCl conditions, it is thought that, as with HNO<sub>3</sub>, they exist as Cu<sup>2+</sup>, but that basic copper chloride was formed by the Cl contained in the solution. Basic copper chloride is also called verdigris and is blue-green in color, so it is thought that verdigris was formed in the Cu+KCl [28].

Comparison of the SEM images showed that P25 had a particle size of less than 50 nm, and Ag particles had a similar size (approximately 50 nm or less) [29,30]. For Cu, no distinct particles were observed, but crystals formed upon drying. W particles ranged from about 50 nm to over 100 nm, displaying no uniformity in particle size. The particles in the Cu+KCl solution were smaller, around 20 nm, compared to P25 and Ag. The particles in the Cu+HNO<sub>3</sub> solution were not spherical but had an irregular shape; a detailed examination of the Cu+KCl solution revealed characteristic particles mixed with nanoparticles. These particles are thought to be derived from Cu<sub>2</sub>O [31]. Therefore, it is suggested that the oxidation state can be controlled by altering the composition of the solution in the liquid plasma.

The EDS spectra of P25 for each treatment condition are shown in Fig. 5A. All samples exhibited elements derived from the metal rod electrodes used in the liquid plasma process. Ag-P25 displayed a higher

peak for Ag compared to the other samples, which can be attributed to its higher content relative to P25. In the case of Cu-P25, trace amounts of Cu ions adhered to the surface of P25 and were precipitated, and trace amounts of Cu were detected [32]. W was also detected in W-P25, but its peak was very small. Among the solutions used to treat P25, the Cu detection was the lowest for the NH<sub>4</sub>OH-treated sample, while the other two conditions showed similar peaks (Fig. 5B). The content of Cu in Cu-P25 relative to P25 decreased as the formed Cu particles dissolved into the NH<sub>4</sub>OH solution. Carbon blacks (CBs) treated under similar experimental conditions displayed the same trend (see [supplementary material](#)).

Table 1 presents the amount of electrode rod material etched, weight ratio (wt%) of electrode rod metal to powder, and the wt% of electrode rod metal to powder calculated from EDS for each treatment condition. Generally, the wt% of electrode rod metal to powder calculated from EDS is underestimated, with the difference being particularly pronounced for NH<sub>4</sub>OH. In the supernatant solution after centrifugation, Ag-P25 contained highly dispersed black particles (see [Supplementary Materials](#)). This solution and Ag-P25 was dissolved in nitric acid and the Ag content was determined by ICP. As a result, the Ag content in P25 was estimated to be 10.5 wt% in powder and 6.2 wt% in solution. As mentioned above, the wt% of Cu to P25 calculated from EDS in the Cu-P25 powder decreased significantly due to the formation of [Cu(NH<sub>3</sub>)<sub>4</sub>]<sup>2+</sup>. The wt% of Cu relative to P25 calculated from the absorption spectrum of [Cu(NH<sub>3</sub>)<sub>4</sub>]<sup>2+</sup> was approximately 7.0 %, which matched the wt% of electrode rod metal. The Cu wt% in the P25 calculated from the EDS was constant for the amount of P25 prepared. In the NH<sub>4</sub>OH solution, Cu is dissolved and does not form discrete particles, leading to its

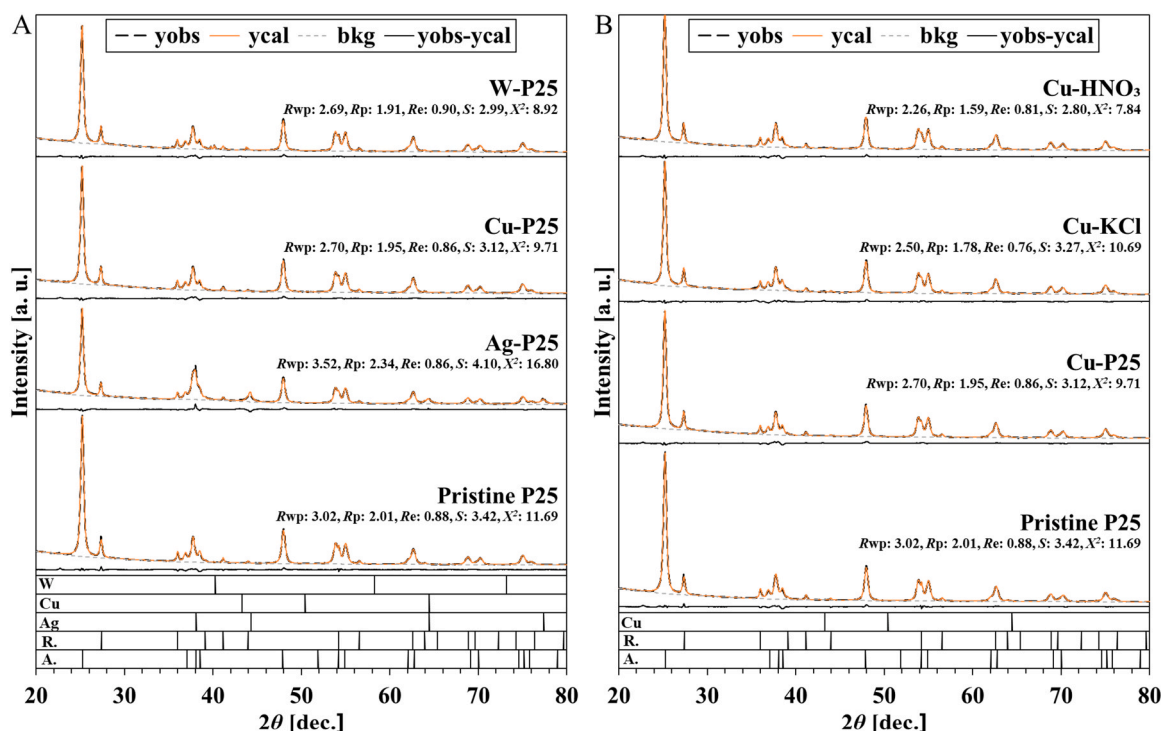


Fig. 6. XRD spectra of P25, Ag-P25, Cu-P25 and W-P25(A), and Cu-P25, Cu-KCl and Cu-HNO<sub>3</sub> (B).

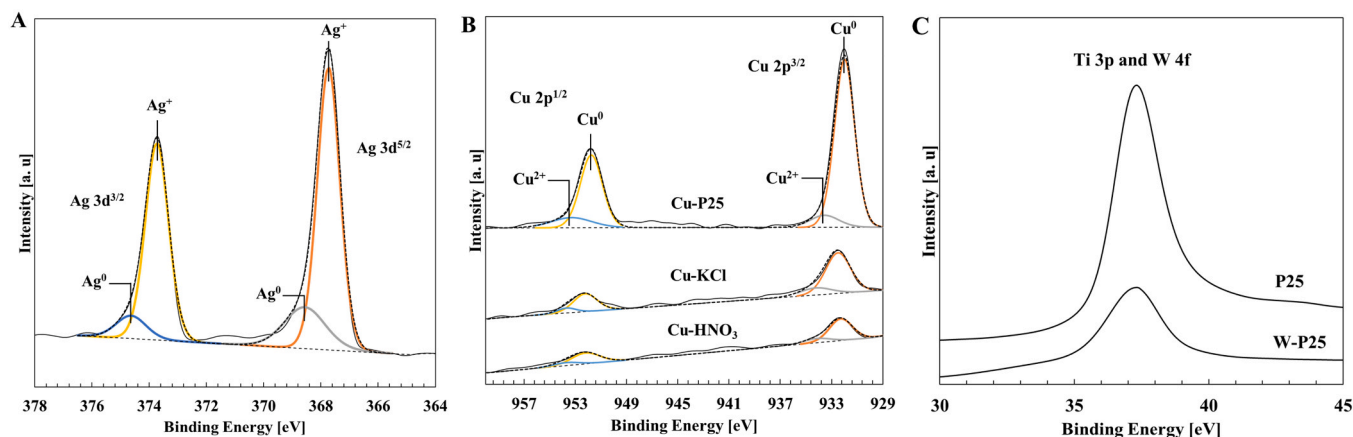


Fig. 7. XPS spectra of Ag 3d of decomposed Ag-P25 (A), Cu 2p of Cu-P25, Cu-KCl and Cu-HNO<sub>3</sub> (B) and Ti 3p and W 4f of P25 and W-P25.

impregnation in P25 depending on the solution concentration. Consequently, the Cu wt% in the P25 calculated from the EDS for Cu-HNO<sub>3</sub> and Cu-KCl treatments is significantly higher compared to that of Cu-P25.

Fig. 6 shows the XRD spectra of P25, Cu-P25, Ag-P25, and W-P25 (A), as well as the Rietveld analysis of P25, Cu-P25, Cu-KCl, and Cu-HNO<sub>3</sub>. The XRD spectra for other samples, including CB, are shown in [supplementary material](#). P25 displays peaks at 25.27°, 37.07°, 38.08°, 38.55°, 47.89°, 54.20°, 54.91°, 62.76°, 69.13°, 70.05°, and 75.19° corresponding to the anatase structure (TiO<sub>2</sub> anatase, CSD: 154061), and peaks at 27.40°, 36.00°, 39.13°, 41.16°, 43.98°, 54.22°, 56.54°, 62.60°, 63.95°, 68.88°, 69.63°, and 76.36° corresponding to the rutile structure (TiO<sub>2</sub> rutile, CSD: 33838). Only Ag-P25 exhibited peaks at 38.12°, 44.31°, 64.45°, and 77.41° which are attributed to Ag (Silver, CSD: 52257). Cu (Copper, ICDD: 00-004-0836) peaks are observed at 43.30°, 50.43°, and 64.45°, while W (Tungsten, ICDD: 00-004-0806) peaks are noted at 40.26°, 58.27°, and 73.20°. However, no peaks were detected in the Cu-P25 and W-P25 sample, possibly due to the detection

Table 2

Lattice constants for each sample obtained from Rietveld analysis.

Sample	Anatase		Rutile	
	a [Å]	c [Å]	a [Å]	c [Å]
Pristine P25	3.7849 (3)	9.5047 (8)	4.5926 (3)	2.9580 (2)
Ag-P25	3.7861 (1)	9.5044 (4)	4.5938 (6)	2.9583 (4)
Cu-P25	3.7862 (1)	9.5060 (2)	4.5940 (4)	2.9585 (3)
W-P25	3.7863 (1)	9.5084 (3)	4.5942 (3)	2.9588 (2)
Cu-KCl	3.7867 (1)	9.5051 (3)	4.5933 (4)	2.9590 (3)
Cu-HNO <sub>3</sub>	3.7871 (1)	9.5065 (3)	4.5940 (3)	2.9587 (2)
Cu-1.0	3.7864 (1)	9.5063 (2)	4.5934 (4)	2.9582 (2)
Cu-2.0	3.7877 (1)	9.5100 (2)	4.5946 (4)	2.9589 (3)

limit of XRD or the presence of non-crystalline amorphous particles. The presence of Ag in Ag-P25 decreased the convergence of the Rietveld analysis. The lattice constants of anatase and rutile crystals for each sample, obtained through Rietveld analysis, are shown in [Table 2](#). This

**Table 3**

Area percentages of decomposed Ag and Cu XPS spectra of Ag-P25, Cu-P25, Cu-KCl and Cu-HNO<sub>3</sub>.

	3d <sup>5/2</sup>		3d <sup>3/2</sup>	
	Ag <sup>+</sup>	Ag <sup>0</sup>	Ag <sup>+</sup>	Ag <sup>0</sup>
Ag-P25	47.7	12.7	34.4	5.2
Cu-P25	58.7	6.0	28.1	7.2
Cu-KCl	58.0	12.7	24.2	5.1
Cu-HNO <sub>3</sub>	49.9	11.4	31.0	7.7

observation suggests that the anatase or rutile crystals may have been impregnated or doped with ions from the metal rod electrodes or oxygen from the liquid plasma [33,34].

The oxidation states of Ag, Cu and W in Ag-P25, Cu-P25, Cu-KCl, Cu-HNO<sub>3</sub>, P25 and W-P25 were evaluated by XPS (Fig. 6 A, B, C). Ag-P25 exhibited a peak at 367 eV corresponding to Ag 3d<sup>5/2</sup> and a peak at 374 eV corresponding to Ag 3d<sup>3/2</sup>. Cu-P25, Cu-KCl, and Cu-HNO<sub>3</sub> showed peaks at 932 eV for Cu 2p<sup>3/2</sup> and 952 eV for Cu 2p<sup>1/2</sup>. The clear peaks observed for Ag-P25 were attributed to its high Ag content. In contrast, Cu-KCl and Cu-HNO<sub>3</sub> had weaker peak intensities compared to Cu-P25, despite similar amounts of Cu being detected by XRD. This suggests that Cu in Cu-P25 was more easily detected due to being

dissolved and highly dispersed in P25. To evaluate the bonding state in detail, the Ag 3d and Cu 2p spectra were deconvoluted. The detailed proportions of Ag and Cu bonding states are provided in Table 3. The Ag 3d<sup>3/2</sup> signal was fitted to two peaks at 367.7 eV and 368.6 eV, corresponding to Ag<sup>+</sup> and Ag<sup>0</sup>, respectively. The Ag 3d<sup>5/2</sup> signal was fitted to two peaks at 373.7 eV and 374.6 eV, also corresponding to Ag<sup>+</sup> and Ag<sup>0</sup>, respectively [35,36]. The Ag<sup>+</sup> signal was dominant, with a proportion of about 80%. This result aligns with the findings of Niu et al., who similarly synthesized Ag nanoparticles in liquid plasma, suggesting that Ag/Ag<sub>2</sub>O nanoparticles with an Ag<sub>2</sub>O surface were also synthesized in this study [37]. For Cu, the Cu 2p<sup>3/2</sup> signal was fitted to two peaks at 932.0 eV and 933.5 eV, corresponding to Cu<sup>0</sup> and Cu<sup>2+</sup>, respectively. The Cu 2p<sup>1/2</sup> signal was fitted to two peaks at 951.8 eV and 953.3 eV, also corresponding to Cu<sup>0</sup> and Cu<sup>2+</sup>, respectively [38,39]. Cu-KCl and Cu-HNO<sub>3</sub> samples showed an increase in the percentage of Cu<sup>2+</sup> from 13% to around 18% compared to Cu-P25, indicating more surface oxidation. Similar to Ag, it can be inferred that Cu/CuO was formed in the Cu samples. From the results of SEM and XPS, it was found that Cu nanoparticles, Cu<sub>2</sub>O and partially oxidized CuO were synthesized by using a Cu rod electrode in in-liquid plasma. W is detected most strongly at W 4f, however, the peak position is very close to Ti 3p. To clarify this, we compared P25 and W-P25, but only the peak intensity decreased, and no change in shape was observed. It is thought that the W 4f peak was buried in the Ti 3p peak due to the low W content.

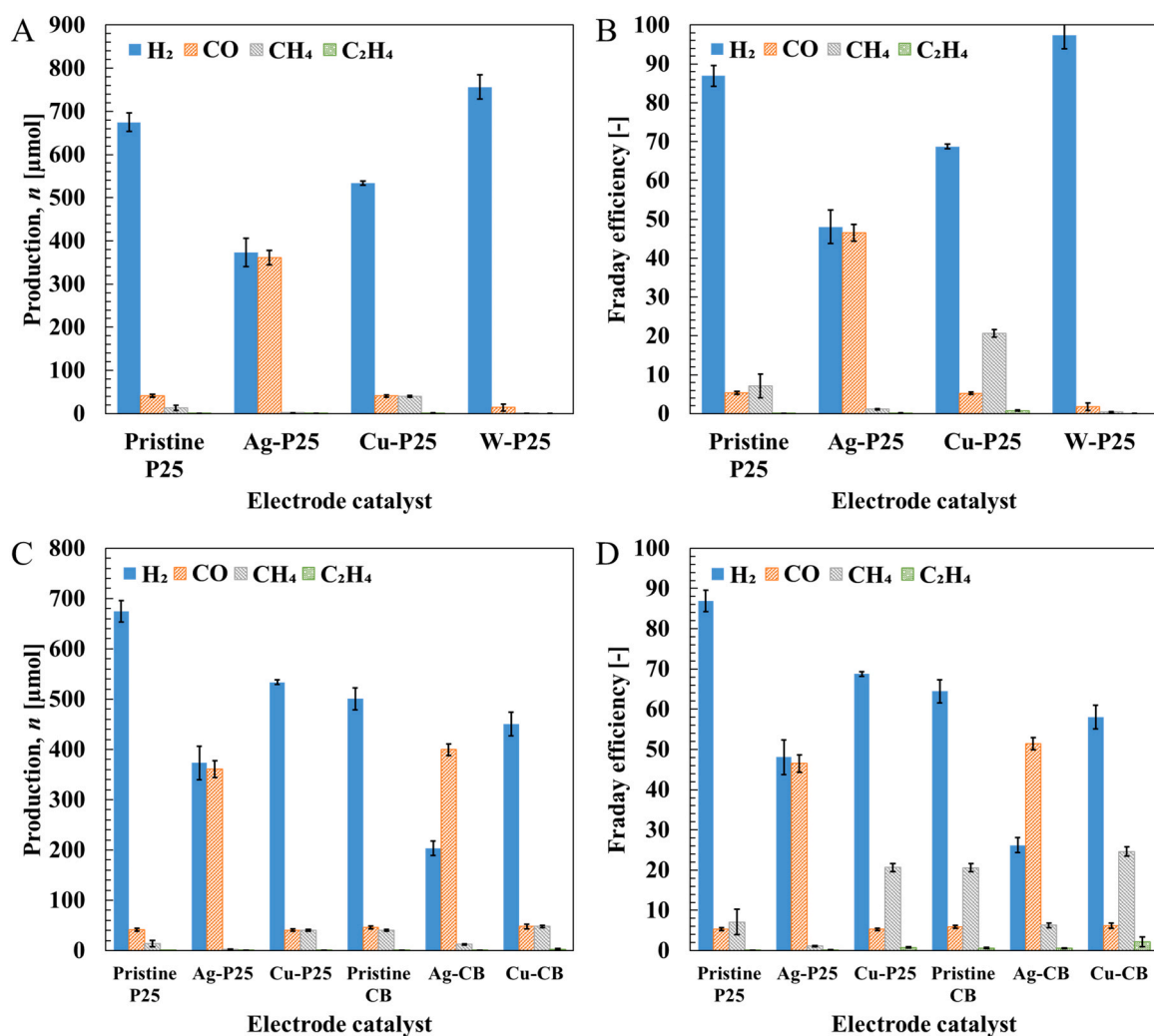


**Fig. 8.** Gas products (A) and faraday efficiency (B) in electrocatalytic CO<sub>2</sub> reduction using P25, Ag-P25, Cu-P25 and W-P25 gas diffusion electrode, and gas products (C) faraday efficiency (D) in electrocatalytic CO<sub>2</sub> reduction products using P25 and CB in-liquid plasma treated under the same conditions sample gas diffusion electrode. The error bars represent the standard deviation of three independent measurements using a new GDE for each measurement.

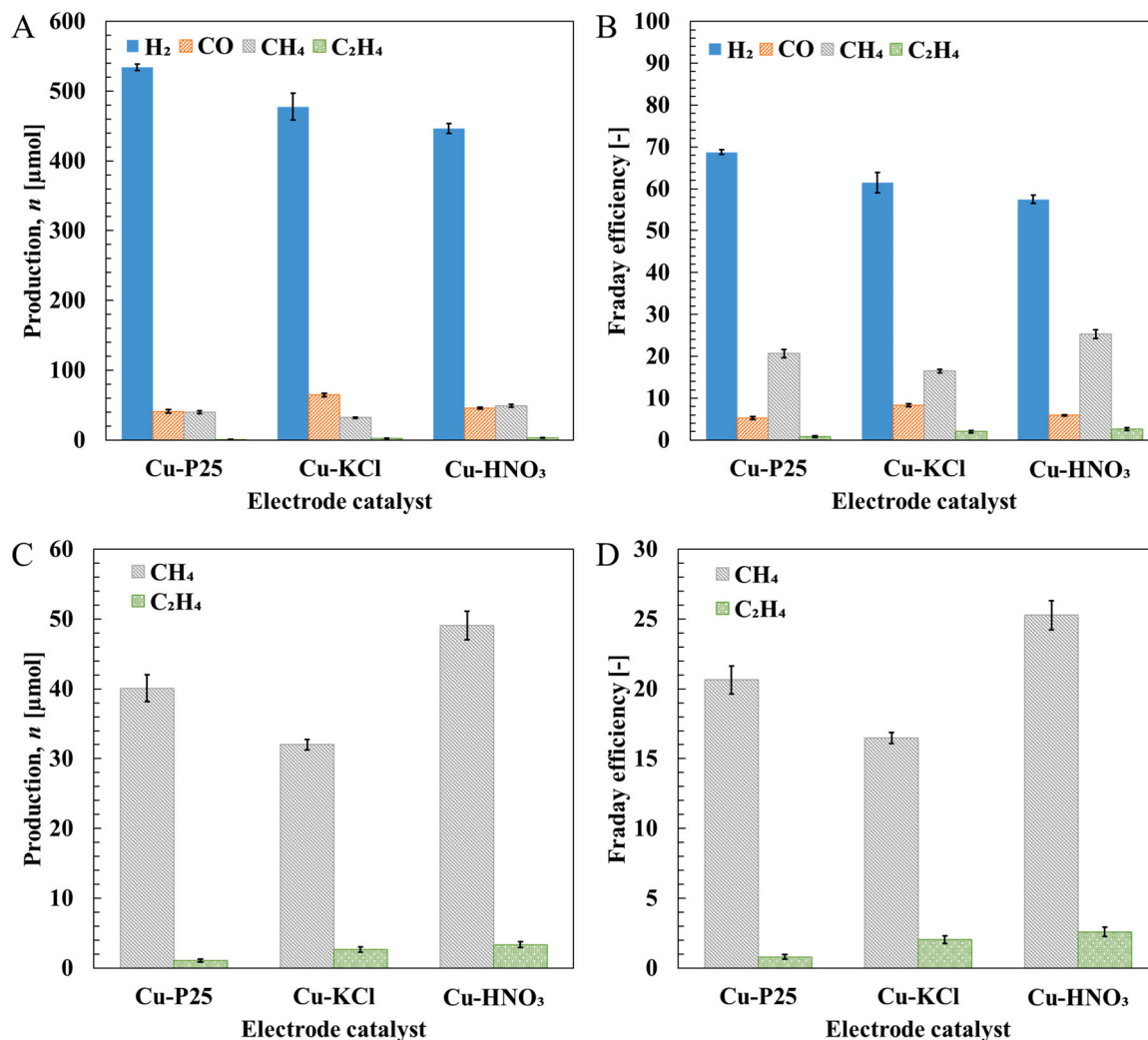


**Fig. 9.** Gas products (A) and Faraday efficiency (B) in electrocatalytic CO<sub>2</sub> reduction, and gas products (C) and Faraday efficiency (D) of hydrocarbon compounds only using Cu-P25, Cu-KCl and Cu-HNO<sub>3</sub> gas diffusion electrodes. The error bars represent the standard deviation of three independent measurements using a new GDE for each measurement.

These findings confirm that nanoparticles derived from metal rods can be synthesized using plasma in liquid. Furthermore, the study demonstrates the potential to control the surface oxidation state of metal nanoparticles through the composition of the solution used in the plasma process.

### 3.2. Evaluation of electrocatalyst CO<sub>2</sub> reduction characteristics

Fig. 8 shows the products (A) and Faraday efficiency (B) of the electrocatalytic CO<sub>2</sub> reduction experiment at a current density of  $-500 \text{ mA/cm}^2$  for P25 in-liquid plasma under various conditions, and the products (C) and Faraday efficiency (D) compared to CB. Detailed information for each sample is provided in [supplementary material](#). As previously reported, unprocessed P25 produced 675 μmol of H<sub>2</sub>, 42 μmol of CO, and 14 μmol of CH<sub>4</sub>, with trace amounts of CO<sub>2</sub> being reduced via the redox cycle of Ti<sup>3+</sup> and Ti<sup>4+</sup> [40]. CH<sub>4</sub> production is attributed to the high hydrogen concentration in the reaction environment at elevated current densities, promoting the multi-electron reduction of CO and hydrogenation [41]. For Ag-P25 and Cu-P25, the main product was H<sub>2</sub>, yielding 360 μmol of CO and 40 μmol of CH<sub>4</sub>, respectively. It has been documented that Ag and Cu can be loaded on TiO<sub>2</sub> to produce CO and CH<sub>4</sub>, a result corroborated in this study [42,43]. In contrast, W-P25 primarily generated 757 μmol of H<sub>2</sub>. This is due to W serving as an active site for water decomposition, enhancing hydrogen production and

inhibiting CO<sub>2</sub> reduction by TiO<sub>2</sub> [14]. Ag-P25 achieved a Faraday efficiency of nearly 50 % for CO, despite containing less than 10 wt% Ag. This efficiency is comparable to that reported for TiO<sub>2</sub> loaded with 5 wt % Ag nanoparticles by Shao et al. [42]. In this study, the partial current density of CO calculated from FE reaches  $-250 \text{ mA/cm}^2$  at a current density of  $-500 \text{ mA/cm}^2$ . It is difficult to make a simple comparison between the amount of Ag nanoparticles loaded on P25 and FE, however, Ag-P25 can maintain a high Faraday efficiency even at high current densities. Yong et al. reported the production of synthesis gas from CO<sub>2</sub> by loading 40 wt% Ag nanoparticles on P25 [44]. Because it is a synthetic gas, the partial current density of CO was evaluated up to  $-164 \text{ mA/cm}^2$  for H<sub>2</sub> and CO at a ratio of 1:2. Generally, the amount of catalyst loaded increases when reducing CO<sub>2</sub> at high current densities. Therefore, Ag-P25 can maintain high CO<sub>2</sub> selectivity at high current densities due to Ag/Ag<sub>2</sub>O. The product trends were similar for both P25 and CB. However, the Faraday efficiency of CB was 10 % lower than that of P25. It has been suggested that CO<sub>2</sub> is reduced to formic acid (HCOOH) when a high voltage is applied to a CB electrode [45,46], indicating conversion to HCOOH. Therefore, synthesizing a catalyst directly on TiO<sub>2</sub> is proposed as a superior method for selectively obtaining desired products.

Fig. 9 shows the products (A) and Faraday efficiency (B) of electrocatalytic CO<sub>2</sub> reduction at a current density of  $-500 \text{ mA/cm}^2$  for Cu-P25, Cu-KCl, and Cu-HNO<sub>3</sub>, as well as the products (C) and Faraday

efficiency (D) of hydrocarbon compounds only. The amount of CH<sub>4</sub> produced was 50 μmol for Cu-HNO<sub>3</sub>, which was more than 1.2 times higher than the 40 μmol for Cu-P25 and 32 μmol for Cu-KCl. The amount of ethylene (C<sub>2</sub>H<sub>4</sub>) produced also increased in the same manner as CH<sub>4</sub>, with Cu-P25 and Cu-KCl producing 1.9 μmol and 2.6 μmol, respectively, and Cu-HNO<sub>3</sub> producing 3.3 μmol. Cu nanoparticles exhibit significantly different CO<sub>2</sub> reduction properties depending on their oxidation state [47,48]. Specifically, oxidized Cu nanoparticles are more effective at reducing CO<sub>2</sub> than unoxidized Cu nanoparticles. This suggests that the surface of Cu-P25 is not oxidized because it was synthesized in NH<sub>4</sub>OH solution. In contrast, Cu-KCl and Cu-HNO<sub>3</sub> were synthesized in neutral or acidic solutions, likely resulting in partial oxidation of the Cu surface, which optimizes it for electrocatalytic CO<sub>2</sub> reduction.

Metal nanoparticles with low oxidation states are synthesized by generating plasma in liquid on a metal rod electrode. These metal nanoparticles immediately react with the solution, which has been activated by the liquid plasma, undergoing either reduction or oxidation. The nature of the solution, particularly whether it is alkaline or acidic, plays a crucial role in determining the outcome. Metal nanoparticles with low oxidation states are reduced in alkaline solutions and oxidized in acidic solutions, indicating that the desired oxidation state can be controlled by the choice of solution.

Moreover, TiO<sub>2</sub> is not entirely dispersed in the solution but exists in a partially aggregated state. It can be inferred that the synthesized nanoparticles are supported on these aggregated TiO<sub>2</sub> structures, resulting in a catalyst with strong physical bonding.

#### 4. Conclusions

The in-liquid plasma synthesis method proved highly effective in incorporating metal particles into TiO<sub>2</sub>, significantly enhancing its electrocatalytic properties for CO<sub>2</sub> reduction. The study found that both the type of metal and its oxidation state critically influence the selectivity and efficiency of the catalytic process.

Ag-P25 demonstrated a remarkable Faraday efficiency of nearly 50 % for CO production, with specific outputs of 360 μmol CO and 40 μmol CH<sub>4</sub>, showcasing its superior catalytic activity. In comparison, Cu-HNO<sub>3</sub> produced 50 μmol of CH<sub>4</sub> and 3.3 μmol of C<sub>2</sub>H<sub>4</sub>, highlighting the importance of copper's oxidation state and treatment method. W-P25 favored H<sub>2</sub> production, yielding 757 μmol, likely due to tungsten's catalytic properties.

These findings underscore the versatility and effectiveness of the in-liquid plasma method for catalyst preparation, allowing for precise control over product distributions in CO<sub>2</sub> reduction. This work lays a robust foundation for future innovations in environmental and energy applications, aiming to reduce greenhouse gas emissions and promote a more sustainable and environmentally friendly economy.

#### CRedit authorship contribution statement

**Chiaki Terashima:** Writing – review & editing, Supervision, Resources. **Izumi Serizawa:** Resources. **Yuvaraj M. Hunge:** Writing – review & editing, Data curation. **Kai Takagi:** Writing – original draft, Methodology, Data curation, Conceptualization.

#### Declaration of Competing Interest

Authors declare that all authors agree to submission and no any interest.

#### Appendix A. Supporting information

Supplementary data associated with this article can be found in the online version at [doi:10.1016/j.jece.2024.115242](https://doi.org/10.1016/j.jece.2024.115242).

#### Data availability

Data will be made available on request.

#### References

- [1] P. Wei, D. Gao, T. Liu, H. Li, J. Sang, C. Wang, R. Cai, G. Wang, X. Bao, Coverage-driven selectivity switch from ethylene to acetate in high-rate CO<sub>2</sub>/CO electrolysis, *Nat. Nanotech.* 18 (2023) 299, <https://doi.org/10.1038/s41565-022-01286-y>.
- [2] Q. Chen, S. Meng, R. Liu, X. Zhai, X. Wang, L. Wang, H. Guo, Y. Yi, Plasma-catalytic CO<sub>2</sub> hydrogenation to methanol over CuO-MgO/Beta catalyst with high selectivity, *Appl. Catal. B: Environ.* 342 (2024), <https://doi.org/10.1016/j.apcatb.2023.123422>.
- [3] Q. Lu, J. Rosen, Y. Zhou, G. Hutchings, Y. Kimmel, J. Chen, F. Jiao, A selective and efficient electrocatalyst for carbon dioxide reduction, *Nat. Commun.* 5 (2014), <https://doi.org/10.1038/ncomms4242>.
- [4] G. Larrazábal, M. Ma, B. Seger, A comprehensive approach to investigate CO<sub>2</sub> reduction electrocatalysts at high current densities, *Acc. Mater. Res.* 2 (2021) 220–229, <https://doi.org/10.1021/accountsmr.1c00004>.
- [5] T. Nguyen, C. Dinh, Gas diffusion electrode design for electrochemical carbon dioxide reduction, *Chem. Soc. Rev.* 49 (2020) 7488–7504, <https://doi.org/10.1039/d0cs00230e>.
- [6] H. Rabiee, L. Ge, X. Zhang, S. Hu, M. Li, Z. Yuan, Gas diffusion electrodes (GDEs) for electrochemical reduction of carbon dioxide, carbon monoxide, and dinitrogen to value-added products: a review, *Energy Environ. Sci.* 14 (2021) 1959–2008, <https://doi.org/10.1039/d0ee03756g>.
- [7] D. Wakerley, S. Lamaison, J. Wicks, A. Clemens, J. Feaster, D. Corral, S. Jaffer, A. Sarkar, M. Fontecave, E. Duoss, S. Baker, E. Sargent, T. Jaramillo, C. Hahn, Gas diffusion electrodes, reactor designs and key metrics of low-temperature CO<sub>2</sub> electrolyzers, *Nat. Energy* 7 (2022) 130–143, <https://doi.org/10.1038/s41560-021-00973-9>.
- [8] M. Monteiro, M. Philips, K. Schouten, M. Koper, Efficiency and selectivity of CO<sub>2</sub> reduction to CO on gold gas diffusion electrodes in acidic media, *Nat. Commun.* 12 (2021), <https://doi.org/10.1038/s41467-021-24936-6>.
- [9] H. Shen, H. Jin, H. Li, H. Wang, J. Duan, Y. Jiao, S. Qiao, Acidic CO<sub>2</sub>-to-HCOOH electrolysis with industrial-level current on phase engineered tin sulfide, *Nat. Commun.* 14 (2023), <https://doi.org/10.1038/s41467-023-38497-3>.
- [10] R. Reske, H. Mistry, F. Behafarid, B. Roldan Cuenya, P. Strasser, Particle size effects in the catalytic electroreduction of CO<sub>2</sub> on Cu nanoparticles, *J. Am. Chem. Soc.* 136 (19) (2014) 6978–6986, <https://doi.org/10.1021/ja500328k>.
- [11] J. Trindell, J. Clausmeyer, R. Crooks, Size stability and H<sub>2</sub>/CO selectivity for Au nanoparticles during electrocatalytic CO<sub>2</sub> reduction, *J. Am. Chem. Soc.* 139 (2017) 16161–16167, <https://doi.org/10.1021/jacs.7b06775>.
- [12] M. Sassenburg, R. de Rooij, N.T. Nesbitt, R. Kas, S. Chandrashekar, N.J. Firet, K. L. Yang, K. Liu, M.A. Blommaert, M. Kolen, D. Ripepi, W.A. Smith, T. Burdyny, Characterizing CO<sub>2</sub> reduction catalysts on gas diffusion electrodes: comparing activity, selectivity, and stability of transition metal catalysts, *ACS Appl. Energy Mater.* 5 (5) (2022) 5983–5994, <https://doi.org/10.1021/acsaem.2c00160>.
- [13] Y. Hattori, S. Mukasa, H. Toyota, T. Inoue, S. Nomura, Synthesis of zinc and zinc oxide nanoparticles from zinc electrode using plasma in liquid, *Mater. Lett.* 65 (2011) 188–190, <https://doi.org/10.1016/j.matlet.2010.09.068>.
- [14] K. Takagi, N. Suzuki, Y. Hunge, H. Kuriyama, T. Hayakawa, I. Serizawa, C. Terashima, Synergistic effect of Ag decorated in-liquid plasma treated titanium dioxide catalyst for efficient electrocatalytic CO<sub>2</sub> reduction application, *Sci. Total Environ.* 902 (2023), <https://doi.org/10.1016/j.scitotenv.2023.166018>.
- [15] B. Sun, M. Sato, J. Clements, Optical study of active species produced by a pulsed streamer corona discharge in water, *J. Electrostat.* 39 (1997) 189–202, [https://doi.org/10.1016/S0304-3886\(97\)00002-8](https://doi.org/10.1016/S0304-3886(97)00002-8).
- [16] Z. Qi, X. Wang, Y. Xia, Z. Zhao, D. Liu, S. Shi, X. Ji, Z. Zhou, The influence of liquid conductivity on pulsed discharge generated by a vertical falling liquid electrode device, *J. Phys. D Appl. Phys.* 55 (2022), <https://doi.org/10.1088/1361-6463/ac9d49>.
- [17] E. Jerby, A. Golts, Y. Shamir, S. Wonde, J. Mitchell, J. LeGarrec, T. Narayanan, M. Sztucki, D. Ashkenazi, Z. Barkay, N. Eliaz, Nanoparticle plasma ejected directly from solid copper by localized microwaves, *Appl. Phys. Lett.* 95 (2009), <https://doi.org/10.1063/1.3259781>.
- [18] I. Ocampo, G. Malapit, R. Baculi, Ar/O<sub>2</sub> atmospheric pressure plasma jet treatment of pure cotton fabric for antibacterial application, *Plasma Fusion Res.* 13 (2018), <https://doi.org/10.1585/pfr.13.3406116>.
- [19] A. Khalil, A. Hafez, M. Elgohary, M. Morsy, Tungsten ion source under double-pulse laser ablation system, *Chin. Phys. B* 26 (2017), <https://doi.org/10.1088/1674-1056/26/9/095201>.
- [20] A. Vesel, R. Zaplotnik, G. Primc, X. Liu, K. Xu, K. Chen, C. Wei, M. Mozetic, Functionalization of polyurethane/urea copolymers with amide groups by polymer treatment with ammonia plasma, *Plasma Chem. Plasma Process.* 36 (2016) 835–848, <https://doi.org/10.1007/s11090-016-9696-3>.
- [21] A. Fierro, G. Laity, A. Neuber, Optical emission spectroscopy study in the VUV–VIS regimes of a developing low-temperature plasma in nitrogen gas, *J. Phys. D Appl. Phys.* 45 (2012), <https://doi.org/10.1088/0022-3727/45/49/495202>.
- [22] Z. Kregar, M. Biscan, S. Milosevic, A. Vesel, Monitoring oxygen plasma treatment of polypropylene with optical emission spectroscopy, *IEEE Trans. Plasma Sci.* 39 (2011) 1239–1246, <https://doi.org/10.1109/TPS.2011.2123111>.
- [23] S. Darwiche, M. Nikravec, S. Awamat, D. Morvan, J. Amouroux, Optical emission spectroscopic investigation of hydrogen plasma used for modification of electrical

- properties of multi-crystalline silicon, *J. Phys. D Appl. Phys.* 40 (2007) 1030–1036, <https://doi.org/10.1088/0022-3727/40/4/017>.
- [24] P. Zheng, S. Li, J. Wang, Evaluation of matrix effects in a pulsed electrolyte cathode atmospheric pressure discharge source for atomic emission, *Anal. Lett.* 51 (2018) 860–869, <https://doi.org/10.1080/00032719.2017.1365266>.
- [25] M. Elsaadany, G. Subramanian, H. Ayan, E. Yildirim-Ayan, Exogenous nitric oxide (NO) generated by NO-plasma treatment modulates osteoprogenitor cells early differentiation, *J. Phys. D Appl. Phys.* 48 (2015), <https://doi.org/10.1088/0022-3727/48/34/345401>.
- [26] J. Liu, X. Wang, X. Li, B. Likozar, A. Zhu, CO<sub>2</sub> conversion, utilisation and valorisation in gliding arc plasma reactors, *J. Phys. D Appl. Phys.* 53 (2020), <https://doi.org/10.1088/1361-6463/ab7c04>.
- [27] B. Yang, X. Tong, Z. Deng, X. Lv, The adsorption of Cu species onto pyrite surface and its effect on pyrite flotation, *J. Chem.* 2016 (2016), <https://doi.org/10.1155/2016/4627929>.
- [28] S. Wolf, C. Feldmann, Cu<sub>2</sub>X(OH)<sub>3</sub> (X = Cl<sup>-</sup>, NO<sub>3</sub><sup>-</sup>): synthesis of nanoparticles and its application for room temperature deposition/printing of conductive copper thin-films, *J. Mater. Chem.* 20 (2010) 7694–7699, <https://doi.org/10.1039/c0jm00681e>.
- [29] S. Jin, S. Kim, S. Lee, J. Kim, Synthesis and characterization of silver nanoparticles using a solution plasma process, *J. Nanosci. Nanotechnol.* 14 (2014) 8094–8097, <https://doi.org/10.1166/jnn.2014.9428>.
- [30] T. Yoshida, N. Yamamoto, T. Mizutani, M. Yamamoto, S. Ogawa, S. Yagi, H. Nameki, H. Yoshida, Synthesis of Ag nanoparticles prepared by a solution plasma method and application as a cocatalyst for photocatalytic reduction of carbon dioxide with water, *Catal. Today* 303 (2018) 320–326, <https://doi.org/10.1016/j.cattod.2017.08.047>.
- [31] C. Kuo, M. Huang, Facile synthesis of Cu<sub>2</sub>O nanocrystals with systematic shape evolution from cubic to octahedral structures, *J. Phys. Chem. C.* 112 (2008) 18355–18360, <https://doi.org/10.1021/jp8060027>.
- [32] M. Behnajady, H. Eskandarloo, Silver and copper co-impregnated onto TiO<sub>2</sub>-P25 nanoparticles and its photocatalytic activity, *Chem. Eng. J.* 228 (2013) 1207–1213, <https://doi.org/10.1016/j.cej.2013.04.110>.
- [33] A. Kuznetsov, R. Machado, L. Gomes, C. Achete, V. Swamy, B. Muddle, V. Prakapenka, Size dependence of rutile TiO<sub>2</sub> lattice parameters determined via simultaneous size, strain, and shape modeling, *Appl. Phys. Lett.* 94 (2009), <https://doi.org/10.1063/1.3139078>.
- [34] A. Garg, A. Singh, V. Sangal, P. Bajpai, N. Garg, Synthesis, characterization and anticancer activities of metal ions Fe and Cu doped and co-doped TiO<sub>2</sub>, *N. J. Chem.* 41 (2017) 9931–9937, <https://doi.org/10.1039/c7nj02098h>.
- [35] S. Ke, C. Kan, Y. Ni, X. Zhu, M. Jiang, C. Wang, X. Zhu, Z. Li, D. Shi, Construction of silica-encapsulated gold-silver core-shell nanorod: Atomic facets enrichment and plasmon enhanced catalytic activity with high stability and reusability, *Mater. Des.* 177 (2019), <https://doi.org/10.1016/j.matdes.2019.107837>.
- [36] U. Sulaeman, S. Suhendar, H. Diastuti, R. Andreas, S. Yin, Design of defect and metallic silver in silver phosphate photocatalyst using the hydroxyapatite and glucose, *Indones. J. Chem.* 20 (2020) 1441, <https://doi.org/10.22146/ijc.48647>.
- [37] Y. Niu, E. Omurzak, R. Cai, D. Kyzy, Z. Zhasnakunov, A. Satyvaldiev, R. Palmer, Eco-friendly synthesis of silver nanoparticles using pulsed plasma in liquid: effect of surfactants, *Surfaces* 5 (2022) 202–208, <https://doi.org/10.3390/surfaces5010013>.
- [38] J. Jiang, X. Liu, J. Han, K. Hu, J. Chen, Self-supported sheets-on-wire CuO@Ni(OH)<sub>2</sub>/Zn(OH)<sub>2</sub> nanoarrays for high-performance flexible quasi-solid-state supercapacitor, *Processes* 9 (2021), <https://doi.org/10.3390/pr9040680>.
- [39] F. Chen, C. Chen, Q. Hu, B. Xiang, T. Song, X. Zou, W. Li, B. Xiong, M. Deng, Synthesis of CuO@CoNi LDH on Cu foam for high-performance supercapacitors, *Chem. Eng. J.* 401 (2020), <https://doi.org/10.1016/j.cej.2020.126145>.
- [40] N. Mendieta-Reyes, W. Chequepán, A. Rodes, R. Gómez, Spectroelectrochemical study of CO<sub>2</sub> reduction on TiO<sub>2</sub> electrodes in acetonitrile, *ACS Catal.* 10 (2020) 103–113, <https://doi.org/10.1021/acscatal.9b02932>.
- [41] G.K. Ramesha, J.F. Brennecke, P.V. Kamat, Origin of catalytic effect in the reduction of CO<sub>2</sub> at nanostructured TiO<sub>2</sub> films, *ACS Catal.* 4 (9) (2014) 3249–3254, <https://doi.org/10.1021/cs500730w>.
- [42] S.C. Ma, Y.C. Lan, G.M.J. Perez, S. Moniri, P.J.A. Kenis, Silver supported on titania as an active catalyst for electrochemical carbon dioxide reduction, *ChemSusChem* 7 (3) (2014) 866–874, <https://doi.org/10.1002/cssc.201300934>.
- [43] A. Anzai, M. Liu, K. Ura, T. Noguchi, A. Yoshizawa, K. Kato, T. Sugiyama, M. Yamauchi, Cu Modified TiO<sub>2</sub> catalyst for electrochemical reduction of carbon dioxide to methane, *Catalysts* 12 (2022), <https://doi.org/10.3390/catal12050478>.
- [44] Y. Kim, B. Kim, W. Lee, Y. Ko, M. Youn, S. Jeong, K. Park, J. Oh, Highly tunable syngas production by electrocatalytic reduction of CO<sub>2</sub> using Ag/TiO<sub>2</sub> catalysts, *Chem. Eng. J.* 413 (2021), <https://doi.org/10.1016/j.cej.2020.127448>.
- [45] J. Wu, T. Sharifi, Y. Gao, T. Zhang, P. Ajayan, Emerging carbon-based heterogeneous catalysts for electrochemical reduction of carbon dioxide into value-added chemicals, *Adv. Mater.* 31 (2019), <https://doi.org/10.1002/adma.201804257>.
- [46] J. Xu, Y. Einaga, Effect of sp<sup>2</sup> species in a boron-doped diamond electrode on the electrochemical reduction of CO<sub>2</sub>, *Electrochem. Commun.* 115 (2020), <https://doi.org/10.1016/j.elecom.2020.106731>.
- [47] A. Zahid, A. Shah, I. Shah, Oxide derived copper for electrochemical reduction of CO<sub>2</sub> to C<sub>2</sub> products, *Nanomaterials* 12 (2022), <https://doi.org/10.3390/nano12081380>.
- [48] F. Roberts, K. Kuhl, A. Nilsson, High selectivity for ethylene from carbon dioxide reduction over copper nanocube electrocatalysts, *Angew. Chem. Int. Ed.* 54 (2015) 5179–5182, <https://doi.org/10.1002/anie.201412214>.